2

CONF-790611--1

SLAC-PUB-2346
June 1979
(A)

MASTER

NEUTRONS FROM MEDICAL ELECTRON ACCELERATORS *

William P. Swanson and Richard C. McCall

Stanford Linear Accelerator Center
Stanford University, Stanford, California 94305

ABSTRACT

The significant sources of photoneutrons within a linear-accelerator treatment head are identified and absolute estimates of neutron production per treatment dose are given for typical components. Measured data obtained at a variety of accelerator installations are presented and compared with these calculations. It is found that the high-Z materials within the treatment head do not significantly alter the neutron fluence, but do substantially reduce the average energy of the transmitted spectrum. Reflected neutrons from the concrete treatment room contribute to the neutron fluence, but not substantially to the patient integral dose, because of a further reduction in average energy. Absolute depth-dose distributions for realistic neutron spectra are calculated, and a rapid falloff with depth is found.

Introduction

There has been recent controversy among radiologists and regulatory agencies in the United States about the seriousness of the risk to patients and hospital personnel arising from unwanted neutrons produced by high-energy therapy accelerators. This paper summarizes recent studies made at SLAC regarding the generation and transport of this neutron field. Although relevance to medical accelerators is emphasized here, these studies are applicable to radiation protection at all electron accelerators which operate above the threshold for photoneutron production.

Neutron Production

The yield of photoneutrons is proportional to the convolution of the (γ,n) cross section and the photon track-length spectrum, which decreases rapidly with photon energy. The result is a yield curve which increases rapidly with primary electron energy for constant electron current up to approximately 25 MeV and more slowly thereafter. For constant electron

* Work supported by the Department of Energy under contract number DE-AC03-76SF00515.

(To be presented at the 3rd All-Union Conference on Applied Accelerators, Leningrad, U.S.S.R., June 25-28, 1979.)

beam power, the neutron yield is almost constant with primary electron energy above 35 MeV. Swanson [Sw78, Sw79] has recently published neutron yield calculations applicable to this energy range (Fig. 1).

In Fig. 2 we have plotted the Monte-Carlo calculated and flattened photon dose rates at a typical 1 meter target distance per mA of electron current for various target thicknesses. The result of dividing the data of Fig. 1 by those of Fig. 2 gives us the ratio of the maximum neutron fluence ϕ_{max} to the useful photon dose at the same distance. This is an absolute prediction to which comparison with measurement is invited. This ratio becomes nearly constant above about 15 MeV incident electron energy where its value is about 7.1×10^6 neutrons cm^{-2} rad^{-1} (Fig. 3). As discussed by examples below,

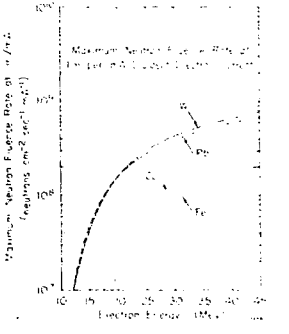

Fig. 1. Calculated maximum neutron fluence rate at 1 m per mA of incident electron current, plotted as a function of electron energy. The conditions for which these curves hold correspond to the case in which all neutron-producing parts are of W or Pb and the movable jaws are fully closed. Isotropic neutron production and no attenuation of neutrons in shielding materials are implicitly assumed. Lower two curves correspond to cases in which all neutron producing parts are made of Fe or Cu and are shown for comparison. Data are derived from Fig. 5 of [Sw79].

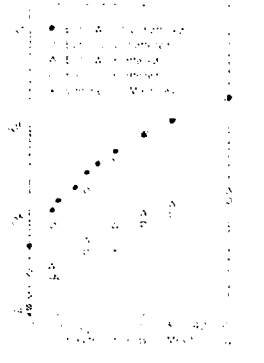

Fig. 2. Photon absorbed-dose index as a function of incident electron energy, as obtained from the Monte-Carlo program EGS. Upper data are from W and Cu targets without flattener. Lower points show same data but after flattening. Measured values obtained on existing commercial accelerators are shown for comparison.

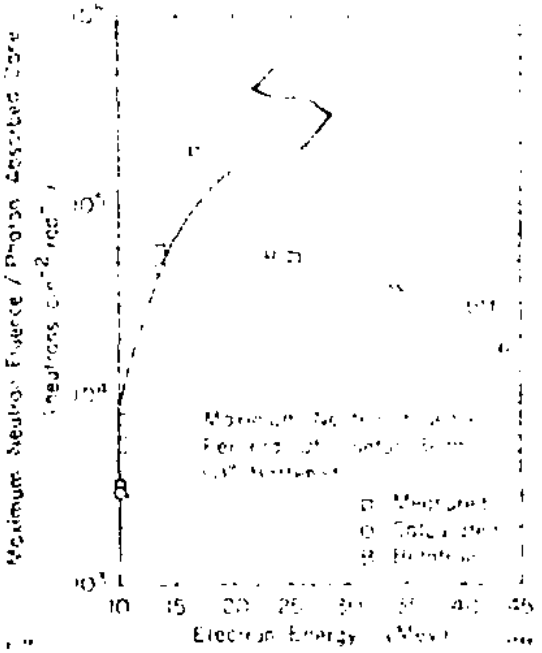

Fig. 3. Maximum neutron fluence per rad of useful beam (0^{0}, flattened). Data are from the W curve of Fig. 1, divided by the photon absorbed dose index for W (flattened) as calculated by the Monte-Carlo program EGS (the triangles of Fig. 2). The conditions for which this curve holds are the same as for Fig. 1. Calculated points (circles) and measured points (squares) are mostly from Table 2.

measured data that [illegible] by below the curve are [illegible] cases in which [illegible] accelerator components are [illegible] high-Z materials, or [illegible] were made with [illegible] Points that fall [illegible] above probably represent cases in which there is substantial [illegible] beam on "targets" within the transport system before it reaches the intended target.

Neutron spectra in the giant resonance contain two components -- the evaporation spectrum and the direct emission spectrum. The evaporation spectrum is the larger component and can usually be described adequately by a Maxwellian distribution

$$\frac{dN}{dE_n} = \left(\frac{E_n}{T^2}\right) \exp\left(\frac{-E_n}{T}\right)$$

where T is the nuclear "temperature" in MeV for the particular nucleus and is also a function of the excitation energy. One should note that the spectrum peaks at $\tilde{E}_n = T$ (most probable energy) and has an average energy of $\bar{E} = 2T$. The evaporation neutrons are emitted almost isotropically. Values of T generally lie in the range 0.5 to 1.0 MeV for high-Z materials. Mutchler has done an extensive study of photoneutron spectra from thin targets [Mu66]. It will be shown later that the spectrum of photoneutrons can be degraded rapidly in heavy metals so published spectra must be considered as representative of a particular target thickness, and this must be taken into account in a proper assessment.

Transport of Neutrons in the Treatment Head

The typical medical accelerator has massive shielding around the target to provide photon shielding and produce a collimated beam of x-rays.

[illegible] approximately [illegible] The [illegible] of lead, [illegible] bending [illegible] mechanism [illegible] and (n,2n) reactions. Both of [illegible] MeV energy region for the (n,2n) [illegible] In both, scattering [illegible] lowest excited state of the shielding material. [illegible] in the neighborhood of 0.6 to 0.8 MeV [illegible] about [illegible] MeV for tungsten; therefore, tungsten is [illegible] in reducing the energy of neutrons by inelastic scattering. In the (n,2n) reaction the minimum energy loss is equal to [illegible] neutron, and since the energies of two emerging neutrons [illegible] to produce large numbers of [illegible] these cross sections together [illegible] neutron energies several million [illegible] In addition, a large amount of elastic scattering [illegible] This results in negligible energy [illegible] increase the path length in the shielding, and [illegible] opportunity for the inelastic and (n,2n) reactions to occur.

Although the spectral [illegible] the attenuation of neutron fluence is small, because the [illegible] cross sections of these materials are small down to [illegible] With a spectrum containing high-energy neutrons, such as [illegible] spectrum, there can, in fact, be a slight build-up of [illegible] due to the (n,2n) reactions. In Figs. 4 and 5 are [illegible] average energy of several spectra calculated after passing through spherical shields of tungsten and lead [Mc78], using the Monte-Carlo [illegible] "MORSE" [St[illegible]]. It can be seen that tungsten reduces the average energy faster than lead, and also that this reduction continues [illegible] depths.

It is frequently stated that a [illegible] spectrum is very similar to the photoneutron spectrum found in [illegible] in this energy range. This is true for the primary spectra, but not for the spectra after they have penetrated the head shielding. In Fig. [illegible] show the integral photoneutron spectra for 15-MeV electrons on tungsten and for ^{252}Cf fission neutrons; these are indeed seen to be quite similar. On the same figure,

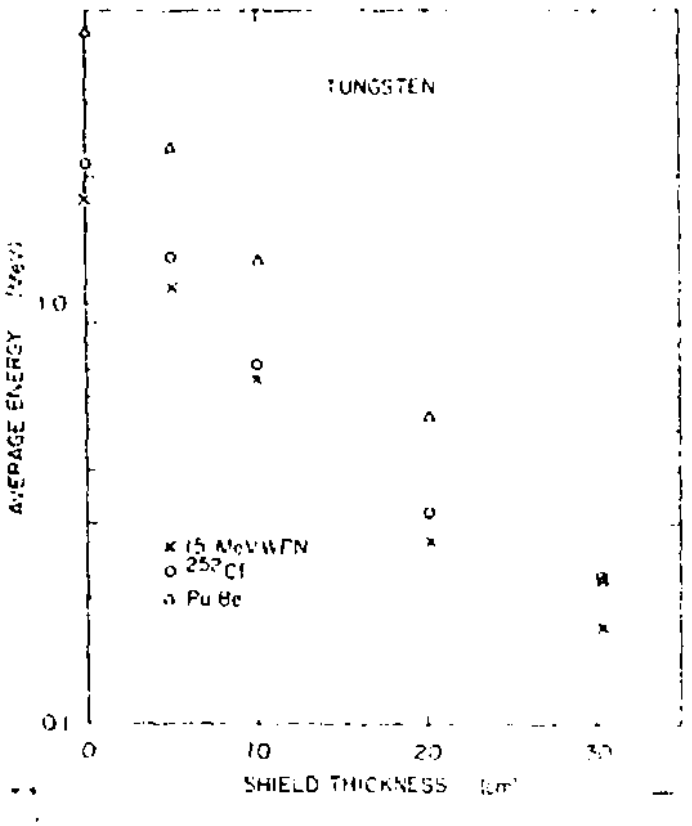

Fig. 4. Average neutron energy as a function of radial W thickness for 15 MeV (incident electron energy) photoneutrons, and ^{252}Cf and PuBe neutron spectra. Over the range of W thickness typically used, there is a substantial decrease in average neutron energy in penetrating the head shielding. Data are from the Monte-Carlo program MORSE.

We show the spectrum from 15 MeV electrons on tungsten after the neutrons have penetrated 10 cm of tungsten. It is clear that there is a large difference between these spectra. In particular, one can see that if one measures the neutrons from a 15 MeV medical accelerator, using a threshold detector calibrated with a bare ^{252}Cf source, the results will be considerably off. Also shown on this figure is the further degradation due to the concrete room in which medical accelerators are commonly placed.

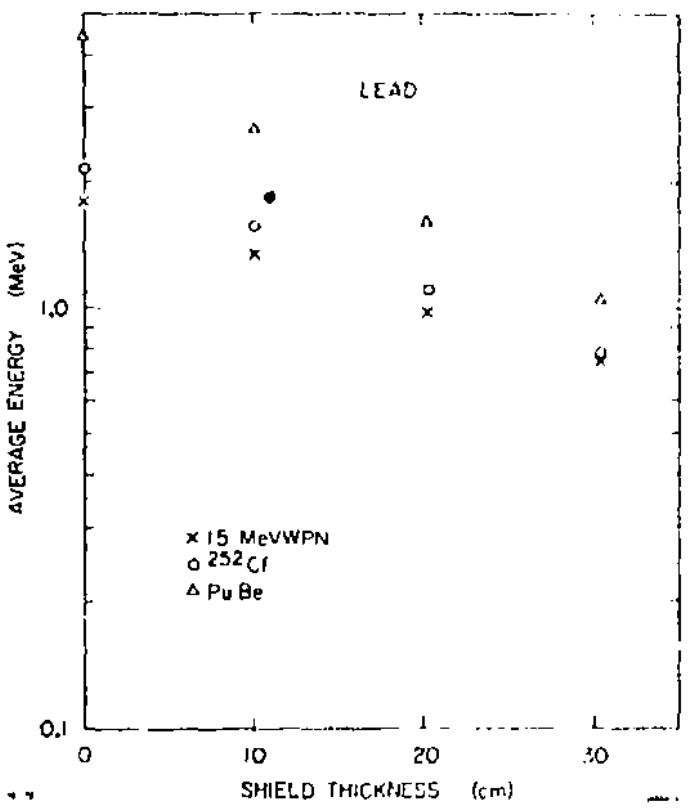

Fig. 5. As for Fig. 4, but for Pb. The reduction in average neutron energy is somewhat less for Pb than for W, even when the two materials are compared on an area-density basis.

Fig. 6. Comparison of various neutron integral spectra to illustrate spectral modification by W shielding and a concrete room. The median energy can be reduced from 1.5 MeV to about 0.2 MeV by the combined effects of the W and concrete. The bare ^{252}Cf spectrum is shown for comparison. Data are from the Monte-Carlo program MORSE.

Neutron Transport in a Concrete Room

Nearly every medical accelerator is placed in a concrete treatment room. In such a room, neutrons from the accelerator scatter in the concrete and may be absorbed or scattered back into the room. These neutrons add to the neutron field arising directly from the accelerator head. However, their contribution to the patient's integral dose is a much smaller fraction of the total, because of the softening of the scattered neutron spectrum discussed above. The average energy of the room-scattered component is about 0.2× of that of the direct component [McGinley, McGinley].

Neutron Sources in a Medical Accelerator

From the calculations of [Swanson, Swanson], one can calculate the neutron yield from a single target material of finite or infinite thickness (≥10 R.L.). It is of interest to compare the neutron yield from an accelerator with these models.

We consider a typical therapy machine with the geometry of Fig. 7. If the target, flattener, jaws and main collimator are of the same material, this would always be Pb or W and, to a reasonable approximation, the neutron yield of these can be considered the same. The only photons effective in producing neutrons are those above about 8 MeV. These are mostly forward directed and will either be absorbed in the main collimator or pass through its opening and through the flattener. Those which penetrate the flattener may or may not strike the jaws, depending on their opening.

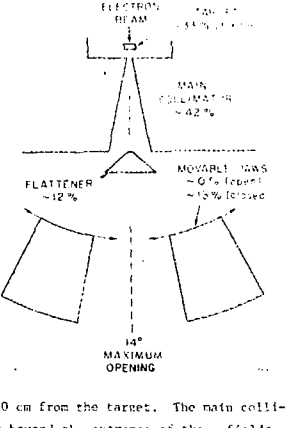

Fig. 7. Arrangement of neutron-producing parts within a radiation treatment unit (not to scale). All of these components are practically indispensible and are found on all standard models. Numbers indicate the approximate percentages of neutrons produced at 25 MeV relative to the maximum number possible, assuming all parts are of high-Z materials (W or Pb).

Those passing through the jaws' opening may be absorbed in the patient, the beam stopper if there is one, or the room concrete. The neutron yield from concrete can be considered negligible, especially since self-shielding would be large.

Most medical linacs provide fields up to about 35 × 35 cm^2 at 100 cm from the target. The main collimator covers all forward directions beyond the extremes of these fields. The half-angle of the main collimator is then about 14 degrees. In order to see what fraction of the high-energy (> 8 MeV) photons are within this angle we have used the Monte Carlo program EGS [Fo78] for various target thicknesses and electron energies. We have used what we believe to be practical linear accelerator target thicknesses. From our Monte-Carlo calculation we can construct curves such as are shown in Fig. 8. As a calculational example consider a 25 MeV accelerator with a 1.0 R.L., W target, W head shielding and a

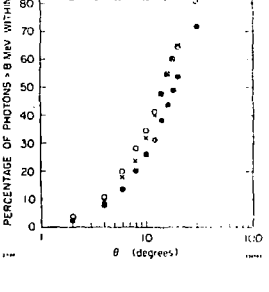

Fig. 8. Percentage of high energy photons (> 8 MeV) emitted within the angle θ from an accelerator target, as a function of θ. Three target material and thickness combinations are shown. Data are based on Monte-Carlo calculations using the program EGS.

W flattener. From Fig. 10 of [Sw78], we find that the neutron yield from this target is about 38% of that for an infinite target. From Fig. 8 we see that the bremsstrahlung is peaked at 0° to the electron beam and 62° outside, so the W flattener with collimator will be practically an infinite absorber. The 25 MeV electrons will strike only the flattener. A target of 0.2 R.L. thickness will be about 2.1 cm (6.6 R.L.) thick in the beam direction. If we model this conical shape with a beam of photons distributed, we effectively have 2.9 R.L. over the central ring. From Fig. 10 of [Sw78] again, we find that these photons produce 47% of the infinite target yield (difference between 1 R.L. and 1 + 2.9 - 1.9 R.L.). Our total neutron yield relative to the infinite target then is as follows:

Target		= 38%
Main Collimator	$= 0.01 \times 0^{2.9}$	= 41.5%
Flattener	$= 0.47 \times 0.38 \times 0.6^{2.9}$	= 12%
Total		= 86.5%

From Fig. 8 of [Sw70] (see Fig. 3), the yield for an infinite target of W at 25 MeV would be 1.5×10^{-3} n/sec per mA. From Fig. 2 we have 8.0×10^{4} rads/min per mA or 60 rads/sec per kW for our example. Then the yield of neutrons relative to the photon output would be 1.5×10^{-3} n/sec-kW $\times$ 0.865 $\div$ 60 rads/sec-kW = 2.16×10^{10} neutrons/rad. This would be the yield with the jaws fully open. Fully closed the yield would be $2.16/0.865 \times 10^{10} = 2.5 \times 10^{10}$ n/rad. With intermediate jaw openings the yield can be calculated by converting the jaw opening to angle and using Fig. 8 to calculate the yield.

We have made similar calculations for several choices of source materials. The results are summarized in Table 1 below. Note that while the

Table 1. Summary of Neutron Source Calculations (25 MeV Electrons).

Material and Percentage of Neutrons				Fraction of Infinite W Yield	Neutrons per rad
Target	Flattener	Main Collimator			
W 38%	W 14%	W 48%		86.5%	2.2×10^{10}
W 43%	Fe 2%	W 55%		64%	1.6×10^{10}
Cu 9.2%	W 30%	W 60.5%		84%	2.1×10^{10}
Cu 12.5%	Fe 5.7%	W 82%		64%	1.6×10^{10}

total neutron yield does not change very much, the fraction of the neutrons originating in different areas changes. This is useful information for an accelerator designer trying to minimize neutron production.

We have made calculations similar to the above for several accelerators for which we have sufficient data on the geometry and materials. In each case, we made measurements of the total fast-neutron source strength (determined by the method described in [Me78] of measuring thermal neutrons in the room) and we have compared our results with these. The results of these calculations are shown in Table 2. These results indicate

Table 2. Calculated and Measured Neutron Yield per Photon rad.

Accelerator	Energy (MeV)	Relative Neutron Yield (n/rad)	
		Calculated	Measured
ATC 25 MeV Betatron	25	6.8×10^{9}	6.9×10^{9}
Siemens 42 MeV Betatron	42	3.8×10^{9}	3.7×10^{9}
Varian Clinac 35 (Old)	25	4.3×10^{10}	8.1×10^{10}
Varian Clinac 35 (New)	25	2.2×10^{10}	6.7×10^{10}
Varian Clinac 18	10	3.9×10^{8}	4.2×10^{8}
Siemens Mevatron XX	15	5.8×10^{9}	7.6×10^{9}

that, in accelerators where the beam losses are reasonably well-known and if target thicknesses and geometries are known, one can probably calculate the neutron yield per photon rad to within ±20%. With these calculations and the "cookbook" methods described in [Me78], one could proceed to calculate the overall head leakage with a total accuracy no worse than about ±50%.

Leakage Neutron Depth-Dose Curves

There has not been very much attention paid to the depth-dose distribution of the leakage neutrons in a patient. It has been shown that these neutrons are of very low energy, and one would expect them to be attenuated quite rapidly in tissue. We have made an attempt to calculate this depth-dose distribution using the computer code MORSE. In the calculation, we have assumed a point source 1 m from the center of the phantom. The source spectrum used was that of either a 14 MeV (incident electron energy) photoneutron spectrum surrounded by 4 inches of tungsten or a 25 MeV photoneutron spectrum surrounded by 4 inches of tungsten. The phantom was a water cylinder one meter long and thirty centimeters in diameter, centered at 1 m from the target perpendicularly to the beam

axis. In Fig. [illegible] dose for the two spectra [illegible]

Fig. 9. [illegible] from the [illegible] electrons.

[illegible]

We have [illegible] neutrons within [illegible] treatment [illegible] fluence [illegible] targets. [illegible] in the [illegible] standard treatment [illegible] neutrons [illegible] by the [illegible] submitted [illegible] the ratio of maximum neutron fluence [illegible] photon dose at the same [illegible]. This ratio rises to an approximately constant value of [illegible] neutrons cm^{-2} rad^{-1} at incident electron energies above 25 MeV. [illegible] we have calculated absolute depth-dose distributions for realistic neutron spectra in H_2O phantoms and found a rapid fall-off with depth.

References

[Fo78] R. L. Ford and W. R. Nelson, "The EGS Code System: Computer Programs for the Monte-Carlo Simulation of Electromagnetic Cascade Showers (Version 3)," Stanford Linear Accelerator Center, Stanford, CA, Report No. SLAC-210 (1978).

[Mc78] R. C. McCall, T. M. Jenkins and R. A. Shore, "Transport of Accelerator Produced Neutrons in a Concrete Room," paper presented at the 5th Conference on Applications of Small Accelerators, held at North Texas State University, Denton, TX, November 6-8, 1978, Stanford Linear Accelerator Center, Stanford, CA, Report No. SLAC-PUB-2214 (1978).

[Mc79] R. C. McCall and W. P. Swanson, "Neutron Sources and their Characteristics," paper presented at the NBS-BRH Conference on Neutrons from Electron Medical Accelerators, Gaithersburg, MD, April 9-10, 1979, Stanford Linear Accelerator Center, Stanford, CA, Report No. SLAC-PUB-2292 (1979).

[Mu66] C. S. Mutchler, "The Angular Distributions and Energy Spectra of Photoneutrons from Heavy Elements," Ph.D. Thesis, MIT, Report No. MIT-2098-224 (1966).

[St76] E. A. Straker, P. N. Stevens, C. C. Irving and V. R. Cain, "The MORSE Code - A Multi-Group Neutron and Gamma-Ray Monte-Carlo Transport Code," Oak Ridge National Lab, Oak Ridge, TN, Report No. ORNL-4585 (1970). Also see Radiation Shielding Information Center, RSIC Computer Code Collection, "MORSE-CG, General Purpose Monte-Carlo Multigroup Neutron and Gamma-Ray Transport Code with Combinatorial Geometry," Radiation Shielding Information Center, Oak Ridge, TN, Report No. CCC-203 (1976).

[Sw78] W. P. Swanson, "Calculation of Neutron Yields Released by Electrons Incident on Selected Materials," Stanford Linear Accelerator Center, Stanford, CA, Report No. SLAC-PUB-2042; and Health Phys. 35, 353 (1978).

[Sw79] W. P. Swanson, "Calculation of Neutron Yields Released by Electrons near the Photoneutron Threshold," Stanford Linear Accelerator Center, Stanford, CA, Report No. SLAC-PUB-2211 (Rev. 1979); and Health Phys., to be published (1979).